Measure and analysis of 4H-SiC Schottky barrier height with Mo contacts

Teng Zhang, Christophe Raynaud, Dominique Planson

Measure and analysis of 4H-SiC Schottky barrier height with Mo contacts

Teng ZHANG, Christophe Raynaud, Dominique Planson
UDL, INSA Lyon, Université Claude Bernard Lyon 1, Ecole Centrale de Lyon, CNRS, Ampère, F-69621, Villeurbanne, France

Abstract – Current-voltage (*I-V*) and capacitance-voltage (*C-V*) characteristics of Schottky Mo/4H-SiC diodes have been measured and analyzed as a function of temperature between 80 K and 400 K. The *I-V* characteristics significantly deviate from ideal characteristics predicted by the thermionic emission model because of the inhomogeneity of Schottky contact. After a brief review of the different existing models, the main parameters (ideality factor, barrier height, effective Richardson constant) of both diodes have been extracted in the frame of a Gaussian barrier height distribution model, whose mean and standard deviation are linearly dependent on voltage and temperature, as well as in the context of the potential fluctuation model. The results are compared with the values extracted by *C-V* and the values in the literature. A link is established between these two models. Diodes of different *I-V* characteristics, either identified as single barrier or double barrier, have been analyzed by DLTS to investigate the deep level defects present. No noticeable difference has been found.

Key-words—Schottky – SiC – I-V – C-V –thermionic-emission – barrier height – DLTS.

1. INTRODUCTION

Since many years, it has been observed that the current-voltage (*I-V*) characteristics of Schottky diodes on SiC are rarely correctly modeled by a simple model of thermionic injection of electrons over a barrier height [1, 2]. This phenomenon is also observed in Schottky on inorganic semiconductor [3]. The thermionic-emission (TE) model gives the forward current I through the diode by the formula:

$$I = AA^*T^2 e^{\frac{-q\Phi_B}{kT}}\left[e^{\frac{q(V-IR_s)}{kT}} - 1\right] \qquad (1)$$

where V is the voltage across the Schottky diode, R_s is its series resistance (including resistance of epitaxial, substrate and back face ohmic contact), A the surface of Schottky contact, A^* the effective Richardson constant, T the temperature, Φ_B the barrier height of the Schottky contact that is assumed constant, q the elementary charge, k the Boltzmann constant. The term preceding the brackets is called saturation current I_s.

In the region where R_s is negligible and $V > 3kT/q$, the relationship can be simplified as:

$$I = I_s e^{\frac{qV}{kT}} \qquad (2)$$

Therefore the plot of $\ln(I)$ *vs.* V should give a straight line whose slope is q/kT and the intercept with y-axis makes it possible to calculate I_s.

In reality, the slope is rarely equal to q/kT and therefore more complex models, ranging from double barrier height models to the Gaussian barrier height distribution as well as models in which Φ_B depends on V and/or T have been published [4-6]. Particularly the Gaussian model explains rather well the measurements made on the Schottky diodes with deposit of Mo on 4H-SiC.

We present an analysis of these different models and apply them to the study of molybdenum Schottky contacts on n-type 4H-SiC epitaxies. The *I-V* and *C-V* characteristics have been measured between 80 and 400 K and the results have been analyzed to extract in particular the barrier heights and ideality factors.

2. ANALYTICAL MODELS

2.1. The ideality factor and the barrier height at 0 V

Considering that the Schottky barrier height (SBH) varies linearly with the voltage as $\Phi_B = \Phi_{B0} + \gamma V$, where Φ_{B0} is the barrier height at 0 V and $\gamma\left(=\partial\Phi_B/\partial V\right)$ is positive, eq. 1 becomes:

$$I = I_s e^{\frac{q(V-IR_s)}{nkT}}\left[1 - e^{\frac{-q(V-IR_s)}{kT}}\right] \qquad (3)$$

with the saturation current I_s given by

$$I_s = AA^*T^2 e^{\frac{-q\Phi_{B0}}{kT}} \qquad (4)$$

where $n = 1/(1-\gamma)$ is recognized as the ideality factor of the diode [7].

According to eqs. 3 and 4, the relationship between $\log(I)$ and V should be linear if the series resistance is small enough to be neglected. Therefore, the ideality factor and the barrier height at 0 V can be determined from the *I-V* plot.

Hackam and Harrop [8] have proposed that, to take into account the effect of a thin interfacial layer as well as the effect

of image force and the presence of surface charges on the barrier height, which also manifest at 0 V and result in $n \neq 1$, it is necessary to integrate the ideality factor into the saturation current as well. Therefore eq. 4 is amended as follows:

$$I_s = AA^*T^2 e^{\frac{-q\Phi_{B0}}{nkT}} \quad (5)$$

2.2. T_0 Effet

In order to precisely fit the experimental *I-V* characteristics of Schottky diodes, where a variation of n with temperature is observed, Padovani and Sumner [9] have suggested to replace T by $T + T_0$ in the thermionic-emission model, therefore eq. 1 becomes (neglecting R_s):

$$I = AA^*T^2 e^{-\frac{q\Phi_{B0}}{k(T+T_0)}}\left[e^{\frac{qV}{k(T+T_0)}} - 1\right] \quad (6)$$

where T_0 neither depends on the temperature nor the voltage over a wide temperature range. Thus, this relation is equal to introduce an ideality factor in the two exponential terms:

$$n = 1 + \frac{T_0}{T} \quad (7)$$

2.3. Gaussian distribution of barrier heights

To explain the difference between SBH measured by *I-V* and *C-V* over the range of measured temperatures, Y. P. Song et al. [4] have assumed that the barrier height is normally distributed with a probability density:

$$P(\Phi_B) = \frac{1}{\sigma_s\sqrt{2\pi}} e^{-\frac{\bar{\Phi}_B - \Phi_B}{2\sigma_s^2}} \quad (8)$$

where $\bar{\Phi}_B$ is the mean barrier height and σ_s is its standard deviation.

As a general SBH distribution, eq. 8 can also be applied at 0 V (the zero bias condition). In that case, the SBH can be expressed as:

$$\Phi_{B0} = \bar{\Phi}_{B0} - \frac{\sigma_{s0}^2}{2kT/q} \quad (9)$$

where $\bar{\Phi}_{B0}$ and σ_{s0} are the corresponding parameters in Gaussian distribution at 0 V. Practically, the SBH at 0 V Φ_{B0} can be calculated at each temperature according to eq. 4 if we know the value of A^*. Thus it is possible to extract $\bar{\Phi}_{B0}$ and σ_{s0} by tracing Φ_{B0} vs. $q/2kT$.

2.4. Potentiel fluctuation model

This model has been developed by Werner and Guttler [5] to explain the temperature dependence of the ideality factor. The barrier height is assumed to be normally distributed, but the mean and standard deviation are assumed to vary linearly with voltage as:

$$\bar{\Phi}_B = \bar{\Phi}_{B0} + \rho_2 V \text{ and } \sigma_s^2 = \sigma_{s0}^2 + \rho_3 V$$

We can then show that the ideality factor can be expressed in the form:

$$\frac{1}{n} - 1 = -\rho_2 + \frac{q\rho_3}{2kT} \quad (10)$$

By tracing $n^{-1} - 1$ *vs.* $q/2kT$, the values of ρ_2 and ρ_3 are obtained respectively from the slope and the y-intercept.

2.5. Flat-band barrier height

Since the barrier height depends on the bias voltage, *i.e.* in fact the electric field, L. F. Wagner *et al.* [6] have proposed to define the barrier height under flat-band condition (zero field) Φ_{BF}, which would be a more fundamental magnitude due to independence of the applied voltage and is given by:

$$\Phi_{BF} = n\Phi_{B0} - (n-1)\frac{kT}{q}\ln\frac{N_C}{N_D} \quad (11)$$

2.6. Richardson plot and its modifications

To determine the effective Richardson constant A^*, the Richardson plot, based on eq. 1 and eq. 2, $\ln(I_S/T^2)$ *vs.* $1/T$ should be linear with a slope related to the barrier height and an intercept bound to A^*.

According to equations 5, 9 and 11, the barrier height is determined from so-called modified Richardson (MR) plots, of which there are several variants.

The plot of $\ln(I_s/T^2)$ *vs.* $1/nT$ (eq.5, [8]), $\ln(I_s/T^2) - q^2\sigma_{s0}^2/2K^2T^2$ *vs.* q/kT (Gaussian model, [10]) or $\ln(I_s/T^2) + (1-1/n)\ln(N_C/N_D)$ *vs.* $1/nT$ ([11]) allow to determine the barrier height at 0 V or in flat band condition.

2.7. C-V characteristics

In the case of a n-type Schottky diode with an uniform doping $N_D - N_A$, the capacitance C is related to the width of the space charge region W:

$$C = \frac{\varepsilon_{sc} A}{W} \quad (12)$$

and W relates to the doping concentration by

$$W = \sqrt{\frac{2\varepsilon_{sc}}{q(N_D - N_A)}(V_I - V_r)} \quad (13)$$

where ε_{SC} is the dielectric permittivity of the semiconductor and V_r the reverse polarization.

If doping is uniform, the tracing of $1/C^2 = f(V_r)$ must be straight, and the intersection V_I with x-axis gives the barrier height Φ_B^{C-V} [12]:

$$\Phi_B^{C-V} = V_I + \frac{kT}{q} + (E_c - E_f) \quad (14)$$

3. Experimental device

Two n-type Mo/4H-SiC Schottky diodes have been characterized and noted (a) and (b). The molybdenum anode is in square shape with a surface area of 2.48 mm². Direct *I-V* measurements have been made by the 4-cable method (Kelvin method) with *Keithley K2410* between 80 K and 400 K with a step of 20 K in a cryostat and under darkness. The *C-V* measurements, between 0 and –5 V, were performed under the same conditions at 100 kHz with a *Keysight E4990A impedance analyzer*. The analysis of the electrically active defects has then been conducted with a *PhysTech FT-1230 HERA DLTS* (High Energy Resolution Analysis Deep Level Transient Spectroscopy) bench between 20 K and 550 K. The reverse-state

voltage is V_R = –10 V and the filling pulse voltage is V_p = –0.1 V for a duration of t_p = 100 µs for all DLTS tests. Depending on the temperature range, the DLTS technique used is either DLTS in current mode (measure of current transients) at low temperature (20 – 170 K), or DLTS in capacitance mode at higher temperature (200 – 550 K) for the propose of optimal precision. In order to avoid an annealing effect under the temperature ramp, a fast preliminary DLTS scan has been carried out on both diodes (from 300 to 550, then back to 300 K for a total of 3 hours).

4. Results and Discussion

4.1. *Forward I-V characteristics*

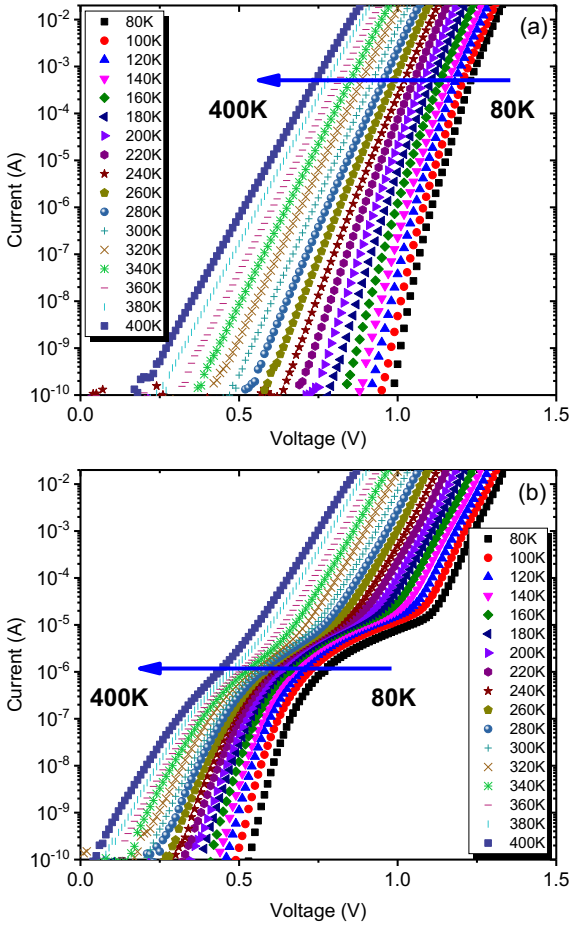

Fig. 1. Forward current-voltage characteristics measured on diodes (a) and (b) of Mo/4H-SiC with a surface area of 2.48 mm^2 between 80 K and 400 K in 20 K increments.

Fig. 1, the log(*I*)-*V* characteristics of the diode (a) are almost linear over the entire temperature range. On the contrary, for the diode (b), the *I-V* curves clearly show a phenomenon of multi-barrier, especially at low temperature. Indeed, under high current (> 10 µA) even at 80 K, log(*I*)-*V* is linear as for diode (b). While under low voltage, the current is abnormally strong compared to the diode (a), although its variation log(*I*) *vs. V* also linear up to about 100 nA. Such multi-barrier behavior has been observed by Gelczuck *et al.* as well [13], who attributed these two parts of the *I-V* curve to an inhomogeneity of the barrier height, a low SBH L-SBH and a higher SBH H-SBH. In that case, the log(*I*)-*V* characteristics can be divided into two linear regions, giving each an ideality factor and a saturation current extracted from eqs 3 and 4.

4.2. *C-V characteristics*

Fig. 2 shows the barrier height and doping concentration extracted from the *C-V* as a function of temperature. Φ_B^{C-V} has a maximum around 200 K. Doping slightly increases with temperature, except for diode (b) at 80 K., which may be due to experimental errors.

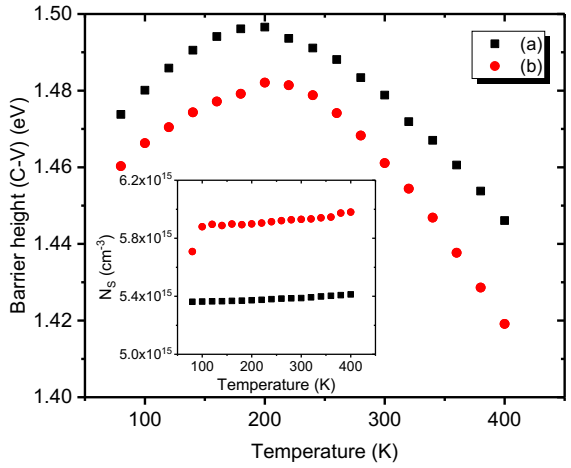

Fig. 2 SBH Φ_B^{C-V} calculated based on the *C-V* characterization. The insert shows the extracted doping concentration.

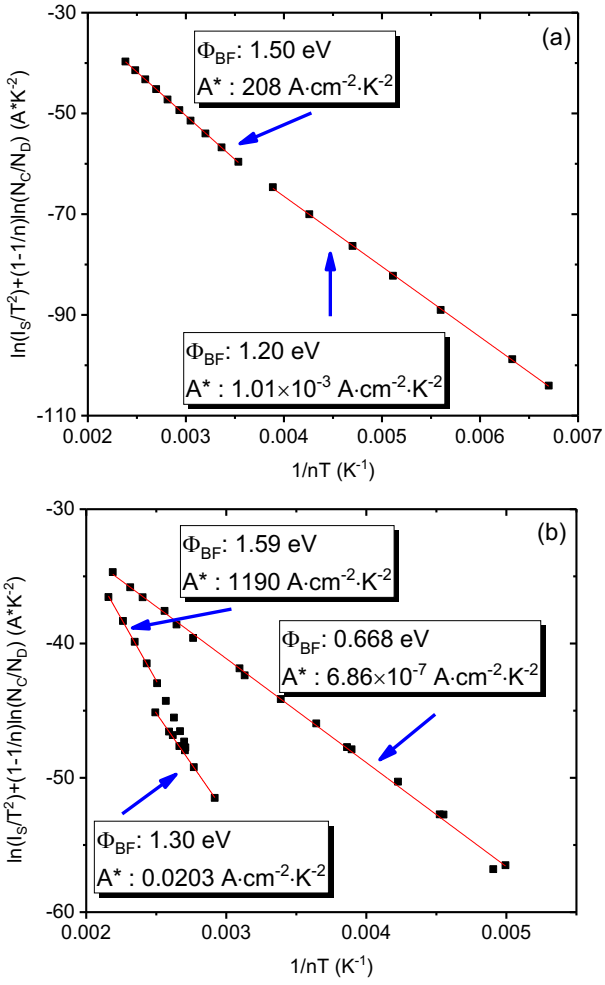

Fig. 3 Modified Richardson plot based on flat-band barrier height on diodes (a) and (b). *n* and I_s were calculated in the different linear zones of the *I-V* curves, and N_D is extracted from the *C-V* characteristics.

4.3. Flat-band barrier height and modified Richardson plot.

The modified Richardson plot based on the flat-band barrier height is adopted here since it is possible to extract all the parameters involved with the *I-V* (n , I_S) and *C-V* curves (N_D).

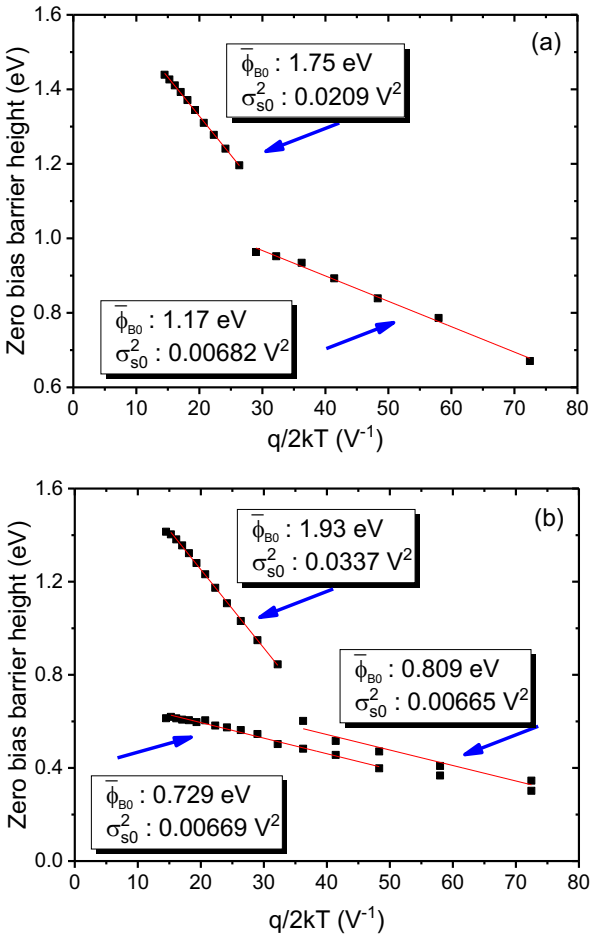

Fig. 4 Barrier heights at 0 V as a function of temperature for extraction of parameters in Gaussian distribution on diodes (a) and (b).

Although *I-V* curves appear linear throughout the temperature range for diode (a), the MR plot [Fig. 3(a)] shows two distinct regions: between 80 and 200 K, Φ_{BF} = 1.20 eV and between 220 and 400 K, Φ_{BF} = 1.50 eV. The diode (b) [Fig. 3(b)] performs similar barrier heights (1.30 eV between 80 and 160 K, and 1.59 eV between 300 and 400 K). However, it also presents a lower barrier height Φ_{BF} = 0.67 eV on the full extent of temperature (80 – 400 K). This lower barrier height is responsible for the excess current at low temperature on (b). A^* has also been calculated in each linear area of the MR plot using the area A of the diode, and the value obtained is used for subsequent calculations. Another solution would be to use a constant value A^* (the higher value extracted, 1.50 eV), and to calculate a ratio between the areas of the high and low SBH regions. The values of A^* are substantially different from several orders of magnitude in different regions, therefore the surface ratio is rather small. Even for a ratio of 5.7×10^{-10} (area of the low SBH on the total surface of the diode), its influence on the *I-V* characteristics cannot be neglected.

For the transition zone between 180 K and 280 K on the diode (b), which can result from the coexistence of two different barriers, the value A^* adopted is that obtained at high temperature.

4.4. Gaussian distribution of barrier height

The curves obtained based on the Gaussian model are linear at each region (Fig. 4). The average value of the barrier height with Gaussian distribution therefore appears as the limit at very high temperature. Consider the common SBH of both diode, for high temperature measurements, $\bar{\Phi}_{B0}$ ~1.8 eV for both while at low temperature $\bar{\Phi}_{B0}$ ~1.17 eV for (a) and ~0.73 eV for (b). The similar H-SBH that dominates at high temperature is close to the barrier that is obtained by *C-V*. Indeed, the barrier height extracted by *C-V* is always that corresponds to the region of greater contact area [4]. At low temperatures, the two diodes have distinct behavior and the barrier heights are different, but their temperature variations (*i.e.* standard deviation σ_s) in each region are still similar. A more remarkable difference for the transition zone between low and high SBH could be due to the value A^* adopted in the high temperature zone.

The disadvantage of this model is that it requires to characterize the distribution of barrier height, and to know the value of A^*, otherwise either using a value from the literature such as Reddy *et al.* [10] or extracting the value from a MR plot (sect. 4.3).

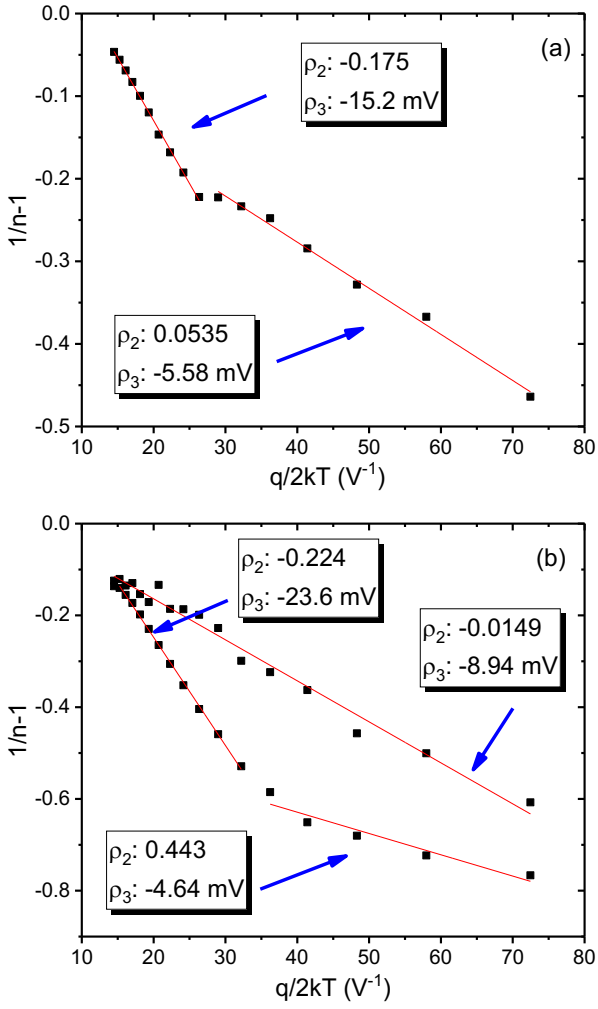

Fig. 5 : Tracing of *1/n-1* in terms of *q/2kT* on the diodes (a) and (b).

4.5. Potentiel fluctuations model

Fig. 5 shows the experimental plot of $n^{-1}-1$ *vs.* $q/2kT$. The values of ρ_2 and ρ_3 are determined from the slope and the intercept. Since the ideality factor n can be obtained directly

from the *I-V* curves, thus it can rule out the error from the value of A^*, unlike in the Gaussian model.

In the same way as for the Gaussian model, linear zones can be identified and the coefficients ρ_2 and ρ_3 are determined in each zone. Referring to the L-SBH, the coefficients ρ_3 are similar for both diodes (~ –5 mV).

4.6. DLTS measurements

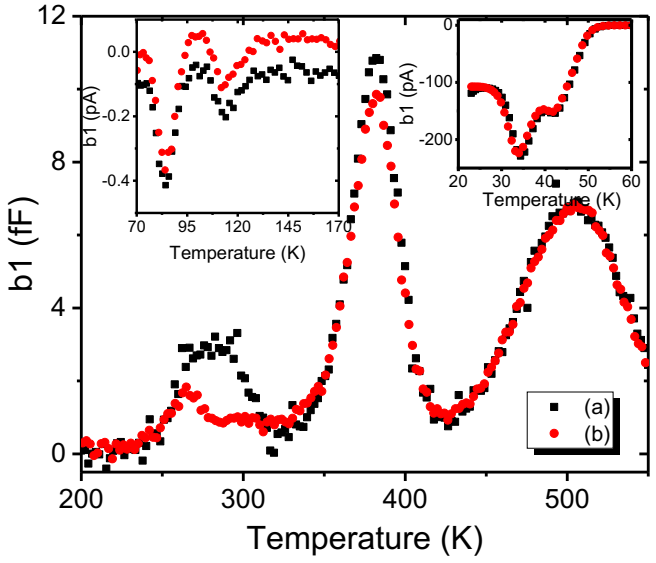

Fig. 6 DLTS signal (correlation b1) with a period of 204.8 ms on the diodes (a) and (b) between 200 K and 550 K. The inserts are current DLTS (I-DLTS) spectrum between 20 K and 60 K (upper right) and 70 K to 170 K (top left). The reverse bias V_R = -10 V, the pulse voltage V_P = -0.1V and the pulse duration t_P = 100 µs for all measures.

Fig. 6 shows the DLTS spectra of the diodes after their *I-V* and *C-V* characterizations between 20 and 550 K. The I-DLTS spectra are dominated by two negative peaks between 70 and 170 K, and two other peaks below 60 K. These defects were analyzed by an Arrhenius plot and their characteristics are gathered in Table 1. The characteristics of other defects that appear on capacitance DLTS spectra are given in Table 2.

Table 1. Charecteristics (activation energy E_C-E_T, capture cross section σ and concentration N_T) obtained by Arrhenius plot of defects detected by I-DLTS (20 K - 170 K). The defects are marked by the peak position of the DLTS signal shown in Fig. 6.

diode (a)				
T (K)	35	42	83	115
E_c-E_t (eV)	0,084	0,087	0,154	0,229
σ (cm²)	1,15E-11	1,09E-13	1,56E-15	8,88E-15
N_T (cm^{-3})	8,16E13	5,26E13	5,33E12	1,42E11
diode (b)				
T (K)	34	43	84	112
E_c-E_t (eV)	0,075	0,083	0,152	0,245
σ (cm²)	1,14E-12	4,90E-14	1,19E-15	3,67E-14
N_T (cm^{-3})	8,13E13	5,24E13	4,86E12	3,58E12

As we can see in Fig. 6, the DLTS results are rather similar between the two diodes, with the only exception of the peak around 280 K. Considering the uncertainties inherent in the Arrhenius analysis, the energies extracted for this peak are quite close to each other, which means that the defects observed are common on the two Mo diodes.

Table 2. Characteristics (E_C-E_T activation energy, capture cross section σ and N_T concentration) obtained by Arrhenius plot of defects detected by C-DLTS (200 K - 550 K). The defects are marked by the peak position of the DLTS signal shown in Fig. 6.

diode (a)					
T (K)	280		380	510	
E_c-E_t (eV)	0,574	0,626	0,839	0,863	0,914
σ (cm²)	1,49E-15	1,84E-15	2,11E-15	1,49E-18	8,87E-18
N_T (cm^{-3})	8,16E11	8,25E11	3,45E12	1,01E12	1,81E12
diode (b)					
T (K)	265	295	383	505	
E_c-E_t (eV)	0,517	0,583	0,813	0,946	0,944
σ (cm²)	2,61E-16	1,12E-16	1,02E-15	8,97E-17	1,58E-17
N_T (cm^{-3})	4,73E11	3,09E11	2,99E12	1,25E12	1,69E12

The physical origin of these defects is specified in Table 3. The two levels at ~ 40 K are attributed to nitrogen. Their activation energies and high concentrations correspond well to the values determined in the literature.

The default at 0.15 eV has been attributed to the Ti [14, 15] or to the Cr [14-16]. However, apart from unintentional contamination during manufacture, it is difficult to relate this level to Cr or Ti.

The defect Z_1/Z_2 is observed around 280 K, with very low concentrations compared to that measured after radiation (*e.g.* by protons [17] or Kr ions [18]).

The origins of deeper defects labeled NB and $RD_{1/2}$ centers are not clear. However, same defect levels detected among Schottky diodes fabricated with various metal contacts on 4H-SiC indicate that their origins are rather related to the SiC than to the metal contact. Similar levels have also been reported by K. Kawahara *et al.* after either high temperature oxidation or C^+ implantation followed by Ar annealing and labeled as ON1 and ON2, where these levels are assumed to originate from the interstitials generated at the SiO_2/SiC interface [19].

Table 3. Identification of defects based on the published results, marked by the temperature of the DLTS peak obtained with a window of 204.8 ms. The range of activation energies indicated is extracted from the Table 1 and Table 2.

T (K)	**E_c-E_t (eV)**	**Identification**	**Références**
34 - 43	0,075 – 0,087	N	[20-22]
83 - 84	0,152 – 0,154	–	–
112 – 115	0,229 – 0,245	Impuretés métalliques	[23]
265 – 295	0,517 – 0,626	Z_1/Z_2	[17, 18, 24, 25]
390 – 393	0,813 – 0,839	NB center	[26]
505 – 510	0,863 – 0,944	$RD_{1/2}$	[17, 24, 27]

5. DISCUSSION

The obtained values of Φ_{B0}, Φ_{BF} and Φ_B^{C-V} on both diodes are represented in Fig. 7. Φ_{B0} varies over the entire temperature range while Φ_{BF} almost remains constant, with values close to

Φ_B^{C-V}. These Φ_{BF} values based on eq. 11 at each temperature are in good agreement with the values obtained by the modified Richardson plot (Fig. 3).

The discontinuity of Φ_{BF} results from the change in value of A^* in both high and low temperature regions. For the diode (b), the difference between Φ_{BF} and Φ_B^{C-V} is slightly larger due to errors in the MR plot or doping extracted by *C-V*.

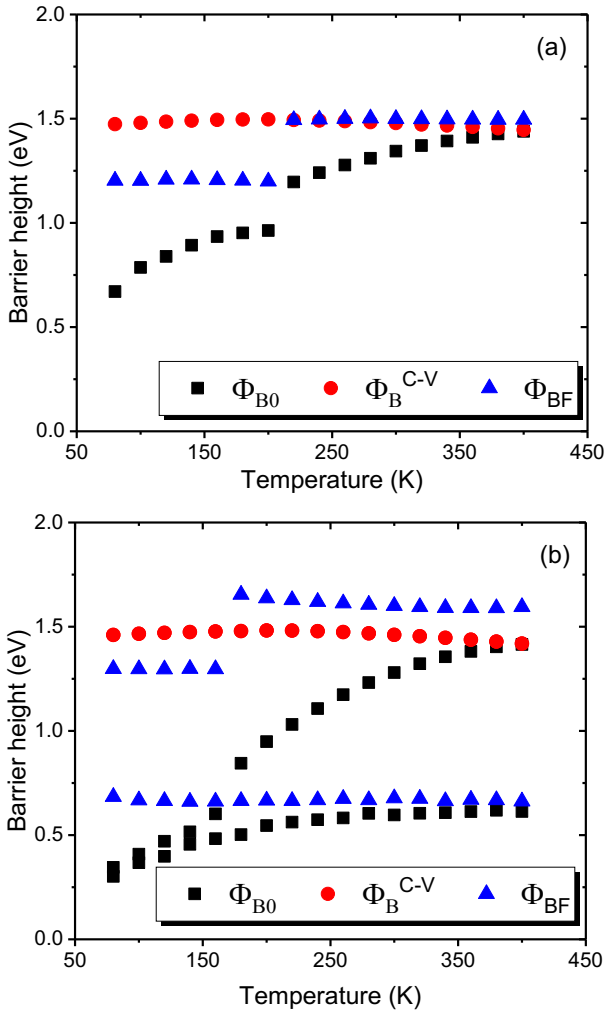

Fig. 7 Temperature evolution of the SBH at 0 V Φ_0 extracted from *I-V*, the SBH extracted from *C-V* Φ_B^{C-V} and the flat-band SBH Φ_{BF} on the diodes (a) and (b).

Consider the T_0 effect where the constant extracted from nT *vs.* T plot with a typical value around 100 K in our case. Therefore eq. 11 is reduced to

$$\Phi_{BF} \approx n\Phi_{B0} \tag{15}$$

since the second part of the expression $\ln(N_C/N_D)kT_0/q$ can be neglected. Equation 15 can well explain the MR plot according to eq. 5, where the value extracted should be close to Φ_{BF}.

Therefore, by replacing Φ_{B0} by Φ_{BF}/n in the eq. 9, the relationship between the ideality factor and and the parameters of the Gaussian distribution can be expressed in the form :

$$\frac{1}{n} - 1 = \frac{\bar{\Phi}_{B0} - \Phi_{BF}}{\Phi_{BF}} - \frac{q\sigma_{s0}^2}{2kT\Phi_{BF}} \tag{16}$$

Comparing with eq. 10, we can show that:

$$\begin{cases} \rho_2 = \dfrac{\Phi_{BF} - \bar{\Phi}_{B0}}{\Phi_{BF}} \\ \rho_3 = -\dfrac{\sigma_{s0}^2}{\Phi_{BF}} \end{cases} \tag{17}$$

or

$$\begin{cases} \bar{\Phi}_{B0} = (1-\rho_2)\cdot\Phi_{BF} \\ \sigma_{s0}^2 = -\rho_3 \cdot \Phi_{BF} \end{cases} \tag{18}$$

This highlights the links between the Gaussian distribution model and the potential fluctuation model. Mean barrier heights and standard deviations calculated according to eq. 18 are given in the Tableau 4, as well as the other parameters used in these two models.

The values between the two models are in good agreement, especially for diode (a). On the diode (b) the slight disagreement could come from either the errors related to the linear approximations of the experimental curves or to the approximation of the eq. 15.

Tableau 4. Comparison of the parameters of the Gaussian model and the potential fluctuation model. Both parameters $\bar{\Phi}'_{B0}$ and σ'^2_{s0} are calculated from the eq. 18 with A^* extracted from the MR trace of the Fig. 3.

Diode	Φ_{BF} (eV)	ρ_2	ρ_3 (mV)	$\bar{\Phi}_{B0}$ (eV)	σ_{s0}^2 (V^2)	$\bar{\Phi}'_{B0}$ (eV)	σ'^2_{s0} (V^2)
(a)	1,50	-0,175	-15,23	1,75	0,021	1,76	0,023
	1,20	0,0535	-5,58	1,17	0,0068	1,14	0,0067
(b)	1,59	-0,224	-23,57	1,92	0,034	1,95	0,037
	1,30	0,443	-4,64	0,81	0,0066	0,72	0,0060
	0,67	-0,0149	-8,94	0,73	0,0067	0,68	0,0060

6. CONCLUSIONS

The two molybdenum-based Schottky diodes have been characterized by *I-V*, *C-V* and DLTS. The modified Richardson plot has been adopted to extract barrier height in flat band condition. This circumvents the weak point of the Gaussian distribution model (which requires knowing the value of A^*) and improves accuracy over the conventional Richardson plot.

Based on the modified Richardson plot, Richardson constants A^* have been determined in each operating region. The SBH models, namely Gaussian distribution and potential fluctuation, have been verified and main parameters have been calculated from the determined A^* values. Both models are in good agreement.

Conventional DLTS and I-DLTS analysis have been performed between 200 and 550 K and between 20 and 170 K to investigate the presence of deep level defects. Four defects have been detected and identified at low temperatures and five at higher temperatures. The Z_1/Z_2 defect is present in small concentration. The origin of high temperature defects is not determined, although they are also listed in the literature.

In any case, no particular difference has been revealed between the two DLTS diodes, which means that the multiple

barrier phenomenon on the *I-V* curves does not originate in the deep level defects, at least in this temperature range studied.

In addition, the approximation of Φ_{BF} as a function of Φ_{B0} and n has been underlined. The result is a link between the Gaussian distribution models and the potential fluctuation model that had not yet been published. The parameters of these two models have been compared using the value of the barrier height in flat band condition, and it appears that the two models are in good agreement.

7. ACKNOWLEDGEMENTS

The authors thank the Chinese government for its financial support through a scholarship from the Chinese Scholarship Council (CSC) no. 201506090154, as well as the National Center of Microelectronics of Barcelona and Caly Technologies for the manufacture/design of the components.

8. REFERENCES

[1] D. Defives, et al., « Barrier inhomogeneities and electrical characteristics of Ti/4H-SiC Schottky rectifiers », IEEE Transactions on Electron Devices, vol. 46, p. 449-455, 1999.

[2] C. Raynaud, et al., « Barrier height determination of SiC Schottky diodes by capacitance and current–voltage measurements », Journal of applied physics, vol. 91, p. 9841-9847, 2002.

[3] S. Bandyopadhyay, et al., « Measurements and modelling of the barrier heights and ideality factors in the metal/conducting polymer composite Schottky device », Journal of applied physics, vol. 85, p. 3671-3676, 1999.

[4] Y. Song, et al., « On the difference in apparent barrier height as obtained from capacitance-voltage and current-voltage-temperature measurements on Al/p-InP Schottky barriers », Solid-State Electronics, vol. 29, p. 633-638, 1986.

[5] J. H. Werner, et al., « Barrier inhomogeneities at Schottky contacts », Journal of Applied Physics, vol. 69, p. 1522-1533, 1991.

[6] L. Wagner, et al., « A note on the correlation between the Schottky-diode barrier height and the ideality factor as determined from IV measurements », IEEE electron device letters, vol. 4, p. 320-322, 1983.

[7] S. Chand, et al., « Evidence for the double distribution of barrier heights in Schottky diodes from I - V - T measurements », Semicond. Sci. Technol, vol. 11, p. 1203-1208, 1996.

[8] R. Hackam, et al., « Electrical properties of nickel-low-doped n-type gallium arsenide Schottky-barrier diodes », IEEE Transactions on Electron Devices, vol. 19, p. 1231-1238, 1972.

[9] F. Padovani, et al., « Experimental Study of Gold - Gallium Arsenide Schottky Barriers », Journal of Applied Physics, vol. 36, p. 3744-3747, 1965.

[10] N. N. K. Reddy, et al., « Barrier characteristics of Pt/Ru Schottky contacts on n-type GaN based on I–V–T and C–V–T measurements », Bulletin of Materials Science, vol. 35, p. 53-61, 2012.

[11] S. Chand, et al., « Current-voltage characteristics and barrier parameters of Pd2Si/p-Si (111) Schottky diodes in a wide temperature range », Semiconductor science and technology, vol. 10, p. 1680, 1995.

[12] E. Rhoderick, et al., « Metal-Semiconductor Contacts. 1988. Clarendon », Oxford, 1988.

[13] Ł. Gelczuk, et al., « Correlation between barrier inhomogeneities of 4H-SiC 1A/600V Schottky rectifiers and deep-level defects revealed by DLTS and Laplace DLTS », Solid-State Electronics, vol. 99, p. 1-6, 2014.

[14] N. Achtziger, et al., « Band gap states of Ti, V, and Cr in 4H–silicon carbide », Applied Physics Letters, vol. 71, p. 110, 1997.

[15] N. Achtziger, et al., « Identification of deep bandgap states in 4H- and 6H-SiC by radio-tracer DLTS and PAC-spectroscopy », Nuclear Instruments & Methods in Physics Research Section B-Beam Interactions with Materials and Atoms, vol. 136, p. 756-762, Mar 1998.

[16] N. Achtziger, et al., « Deep levels of chromium in 4H-SiC », Materials Science and Engineering B-Solid State Materials for Advanced Technology, vol. 46, p. 333-335, Apr 1997.

[17] D. V. Davydov, et al., « DLTS study of defects in 6H-and 4H-SiC created by proton irradiation », Physica B-Condensed Matter, vol. 308, p. 641-644, Dec 2001.

[18] E. Kalinina, et al., « Electrical study of 4H-SiC irradiated with swift heavy ions », 2002.

[19] K. Kawahara, et al., « Analytical model for reduction of deep levels in SiC by thermal oxidation », Journal of Applied Physics, vol. 111, p. 053710, 2012.

[20] F. Nava, et al., « Radiation detection properties of 4H-SiC Schottky diodes irradiated up to 10(16) n/cm(2) by 1 MeV neutrons », Ieee Transactions on Nuclear Science, vol. 53, p. 2977-2982, Oct 2006.

[21] E. Omotoso, et al., « Electrical characterization of defects introduced during electron beam deposition of W Schottky contacts on n-type 4H-SiC », Materials Science in Semiconductor Processing, vol. 51, p. 20-24, 2016.

[22] T. Kimoto, et al., « Nitrogen donors and deep levels in high-quality 4H–SiC epilayers grown by chemical vapor deposition », Applied Physics Letters, vol. 67, p. 2833, 1995.

[23] A. Uddin, et al., « Investigation of deep levels and residual impurities in sublimation-grown SiC substrates », Japanese Journal of Applied Physics Part 2-Letters, vol. 33, p. L908-L911, Jul 1994.

[24] T. Dalibor, et al., « Radiation-induced defect centers in 4H silicon carbide », Diamond and Related Materials, vol. 6, p. 1333-1337, Aug 1997.

[25] Z. Q. Fang, et al., « Characterization of deep centers in bulk n-type 4H-SiC », Physica B-Condensed Matter, vol. 308, p. 706-709, Dec 2001.

[26] M. Kato, et al., « Optical cross sections of deep levels in 4H-SiC », Journal of Applied Physics, vol. 100, p. 053708, 2006.

[27] K. Danno, et al., « Midgap levels in both n- and p-type 4H–SiC epilayers investigated by deep level transient spectroscopy », Applied Physics Letters, vol. 86, p. 122104, 2005.